Scanning Microscopy

Volume 7 | Number 4 Article 1

11-18-1993

Cross-Sections for Electron Scattering Accompanied by Ionization of Inner-Shells

M. Kotera
Osaka Institute of Technology

K. Yamamoto
Osaka Institute of Technology

H. Suga
Osaka Institute of Technology

Scanning Microscopy, Vol. 7, No. 4, 1993 (Pages 1135-1144)
Scanning Microscopy International, Chicago (AMF O'Hare), IL 60666 USA

0891-7035/93$5.00+.00

CROSS-SECTIONS FOR ELECTRON SCATTERING ACCOMPANIED BY IONIZATION OF INNER-SHELLS

M. Kotera*, K. Yamamoto, and H. Suga
Osaka Institute of Technology, Omiya, Asahi-ku, Osaka 535, Japan

(Received for publication May 8, 1993, and in revised form November 18, 1993)

Abstract

A method is presented to describe the electron scattering process at an ionization of inner-shell electrons. The differential cross-section with the energy transfer and the momentum transfer is calculated using the expression of the generalized oscillator strength. This cross-section and the total ionization cross-section are fairly close to the results obtained by the Gryzinski equation. The photo-absorption cross-section obtained by the present treatment shows good agreement with the experimental data in a wide range of the photon energy. Based on the present treatment, the scattering angle distribution of the primary electron is calculated.

Key Words: Ionization of inner-shell electrons, ionization cross-section, Hartree-Slater atomic wave function, generalized oscillator strength, photo-absorption cross-section

*Address for correspondence:
M. Kotera,
Department of Electronic Engineering,
Osaka Institute of Technology,
5-16-1 Omiya, Asahi-ku,
Osaka 535, Japan

Telephone number: 81 6-952-3131
FAX number: 81 6-957-2136
e-mail: farkd02@jpnoit20.bitnet

Introduction

Electron scattering phenomena have been simulated in various ways [3, 9-11, 19, 21]. Since the ionization cross-section of inner-shell electrons is not large in the keV energy region compared to that of the conduction electrons or the excitation cross-section of the bulk plasmon, kinematics of electron scattering with the inner-shell electron ionization has been treated rather roughly. For example, in a calculation of a diffusion range of an electron beam in solids, contribution of the inner-shell electron ionization to the angular scattering is less important. The major process of the angular scattering is attributed to the elastic scattering, and the process of the energy loss can be expressed by the continuous slowing down approximation. Namely, it is possible to simulate the diffusion range by the so-called single scattering model of electrons [19], which is based on the screened Rutherford equation for the elastic scattering and the Bethe equation for the energy loss, with considerably high accuracy.

However, in a quantitative discussion of an angular resolved electron energy loss spectrum, not only the inner-shell ionization process but also other major inelastic processes should be treated precisely to interpret characteristic variations of the spectrum. There are some simulation models, which take into account some elemental inelastic scattering processes [3, 11]. It may be possible to use an experimental energy loss function [2], because it automatically includes all processes which electrons undergo. In order to explain the energy loss spectrum at a certain angular deflection, it is necessary to accurately treat the momentum transfer at each inelastic collision. A large momentum transfer results in a large angular deflection of the primary electrons. Inelastic collision processes have been frequently simulated by a classical binary collision model [21]. In the classical treatment, however, if an amount of the energy transfer is fixed, the scattering angle is determined by one angle. On the other hand, in a quantum-mechanical treatment the momentum transfer has a distribution even at a fixed energy transfer, as described by the generalized oscillator strength (GOS).

Symbol Table

π:	= 3.14159
h:	the Planck constant
c:	speed of light
a_0:	Bohr radius
m:	mass of an electron
v:	the initial velocity of the primary electron
$\Re$:	the Rydberg energy = 13.60 eV
$\sigma_{0\eta}$:	The ionization cross-section based on the first Born approximation. 0 and η are the initial and the final state, respectively.
$F_{0\eta}(k)$:	the inelastic form factor
k:	the momentum transfer at one collision
E:	the kinetic energy of the primary electron
E_l:	the energy loss of the primary electron at the collision
$U(r)$:	atomic potential
ϵ_{nl}:	eigen energy of the nl-th sub-shell electrons; negative value
ϵ:	energy of the ionized electron; positive value
$P_{nl}(r)$:	eigen function of the nl-th sub-shell electrons
$P_{\epsilon l'}(r)$:	normalized wave function of the ionized electrons
$j_\lambda(kr)$:	the λ-th Bessel function
$f_{nl,\epsilon l'}(k)$:	the GOS for a transition from nl-th sub-shell to a continuum state with an energy of ϵ.
$\sigma_{nl,\epsilon l'}$:	the ionization cross-section for a transition from nl-th sub-shell to a continuum state with an energy of ϵ and with an angular momentum of l'.
$\sigma_{nl,\epsilon}$:	differential cross-section of the ionization for a transition from nl-th sub-shell to the continuum state with an energy of ϵ.
σ_{opt}:	photo-ionization cross-section for nl-shell electrons
θ:	the scattering angle of the primary electron at the collision
θ_1:	scattering angle of the primary electron
θ_2:	scattering angle of the ionized electron from a direction of the primary electron
E_B:	binding energy of an inner-shell electron
E_i:	energy of the primary electron
E_1:	energy of the scattered primary electron
E_2:	energy of the ionized electron
E_t:	energy loss of the primary electron

The GOS has been originally introduced by Bethe and the work has been intensively summarized by Inokuti in 1971 [8]. Because of the recent computer advancements, the complicated equations can be solved accurately with less approximations. Manson [15] and McGuire [17] have introduced procedures to calculate the GOS with the Hartree-Slater type one-electron wavefunction. Following their work [15, 17], such calculations have been carried out by Scofield [22], Leapman *et al.* [13], Rez [22], Ahn and Rez [1], and Luo and Joy [14]. Since the GOS describes the inner-shell electron ionization, it can be applied to estimate the intensity of a characteristic X-ray generated by electron beam irradiation. Kotera *et al.* [12] have given generation functions of several characteristic X-rays in solids using the GOS.

Here, we present a procedure to calculate the GOS. This procedure is essentially the same as that of Manson's [15] with a little modified expression. We introduce first, the wave function of inner-shell electrons and the atomic potential of a free atom at the ground state. Next, we describe a method to calculate the GOS. Based on the GOS, we obtain the differential and the total ionization cross-sections and the photo-absorption cross-section in solids. They are evaluated by comparisons with other theoretical or experimental data. Finally, based on both the momentum transfer and the energy transfer at the collision, the scattering angle distribution of the primary electrons is shown for a certain energy transfer at the collision.

Theory

Atomic potential

The atomic potential at the ground state used in the present study is the so-called Hartree-Slater potential given by Herman and Skillman [6]. This is a simplified Hartree-Fock potential, derived on the assumption that the electron exchange effect between each sub-shell electron can be substituted by a single mean potential which is calculated by the free-electron gas model. The Hartree-Slater potential and the Hartree-Fock potential are compared in Figure 1 for Al and Cu as a function of the radial distance from the center of the atom. The Hartree-Fock potential is quoted from a paper of Strand and Bonham [24]. It is found that both potentials are fairly close. The eigen value of each sub-shell for C, Al, Si, and Cu atoms in the Hartree-Slater model is summarized in Table 1, and compared with the experimental value of the binding energy quoted from Jolly *et al.* [7]. The difference is less than 10 percent for every sub-shell. The eigen function for each sub-shell electron is used as the initial state in the later calculation of ionization cross-sections.

Generalized oscillator strength

Here, a quantum-mechanical treatment is used for an inner-shell electron ionization by electrons, which has been discussed by Manson [15]. The ionization cross-section of an atom for fast electrons is given by the following equation at the first Born approximation:

$$\sigma_{0\eta} = \frac{8\pi a_0^2}{m v^2/\Re} \int_{\ln(k_{\min} a_0)^2}^{\ln(k_{\max} a_0)^2} \frac{\left| F_{0\eta}(k) \right|^2}{(k a_0)^2} d\ln(k a_0)^2 \qquad (1)$$

where v is the initial velocity of an incident electron, and subscripts 0 and h of $\sigma_{0\eta}$ express the initial and the final state of the atom, respectively. $\Re$ is the Rydberg energy and k is the momentum transfer. $k_{\min}$ and $k_{\max}$ are the minimum and the maximum momentum transfer at the collision. The inelastic form factor is expressed by:

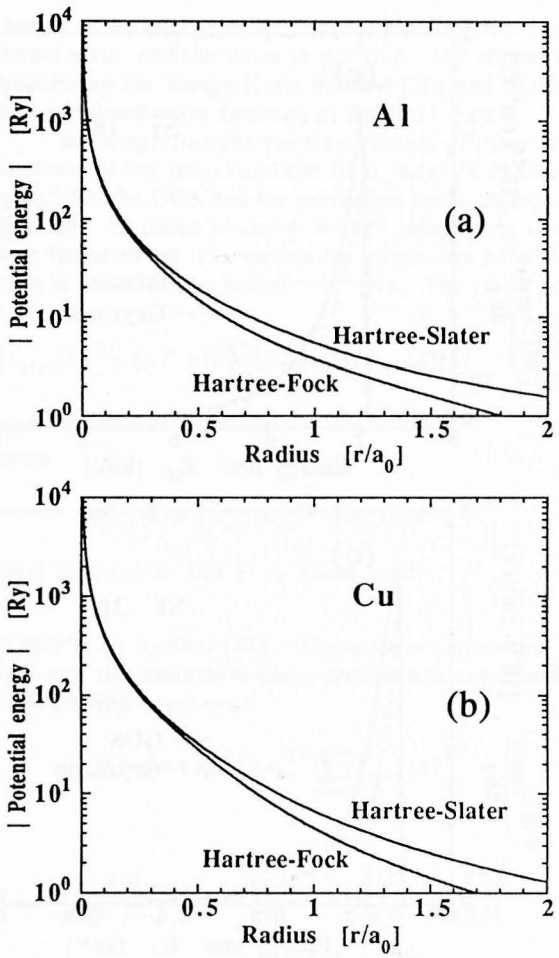

Figure 1. A comparison between the Hartree-Slater and the Hartree-Fock potentials for (**a**) Al and (**b**) Cu atoms as a function of the atomic radius.

Table 1. The binding energy of inner-shell electrons obtained by the Hartree-Slater wave function is compared to the experimental data.

Element		1s	2s	2p	3s	3p
C	Calc.	290.8	17.53			
	Exp.	284.1		7		
Al	Calc.	1545	118.4	80.77		
	Exp.	1560	118.3	73.3		
Si	Calc.	1822	150.7	108.1		
	Exp.	1839	149.3	99.3		
Cu	Calc.	8832	1062	938.3	117.4	77.62
	Exp.	8979	1096	937.7	120	74

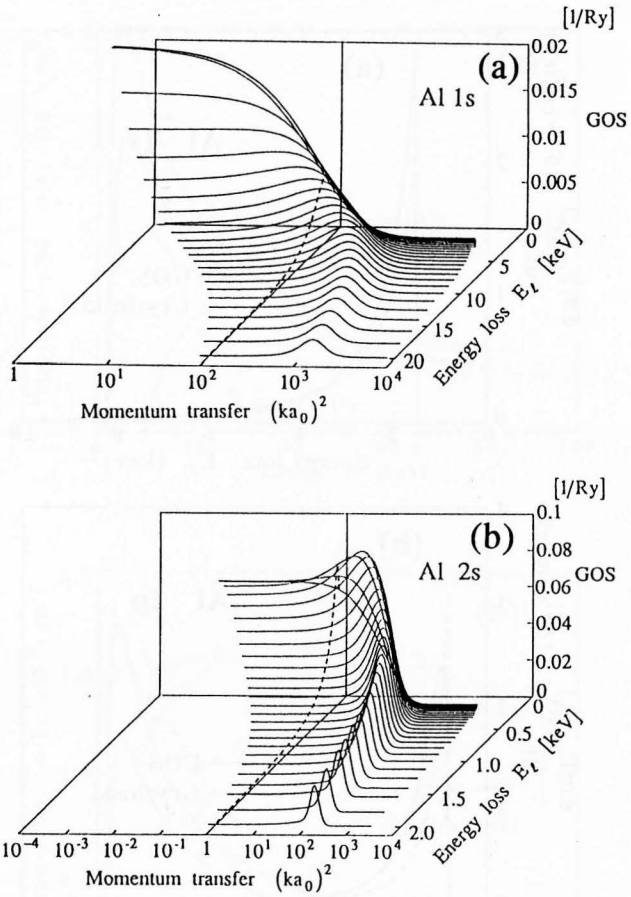

Figure 2. The two-dimensional plot of the GOS, known as the Bethe surface, for (**a**) Al-1s and (**b**) Al-2s electrons as functions of $\ln(ka_0)^2$ and E_l.

$$F_{0\eta}(k) = \left\langle \eta \left| \sum_j e^{i\vec{k}\cdot\vec{r}_j} \right| 0 \right\rangle \tag{2}$$

where $\vec{r}_j$ corresponds to the position vector of j-th electron to the colliding object. The momentum transfer squared is determined by the following equation:

$$(k\,a_0)^2 = 2\,\frac{E}{\Re} - \frac{E_l}{\Re} - 2\left\{\frac{E}{\Re}\left(\frac{E}{\Re} - \frac{E_l}{\Re}\right)\right\}^{1/2}\cos\theta \tag{3}$$

where, θ is the angle of scattering of the primary electron, E_l (= E - E_0) is the loss energy of the primary electron, and E {= $(mv^2)/2$} is the kinetic energy of the primary electron. The integration limits $(K_{max}a_o)^2$ and $(K_{min}a_o)^2$ are determined from eq. (3) with $\theta = \pi$ and $\theta = 0$. Using the inelastic form factor, the GOS is expressed by the following equation:

$$f_{0\eta}(k) = \left(E_\eta - E_0\right)\left(k\,a_0\right)^{-2}\left|F_{0\eta}(k)\right|^2 \tag{4}$$

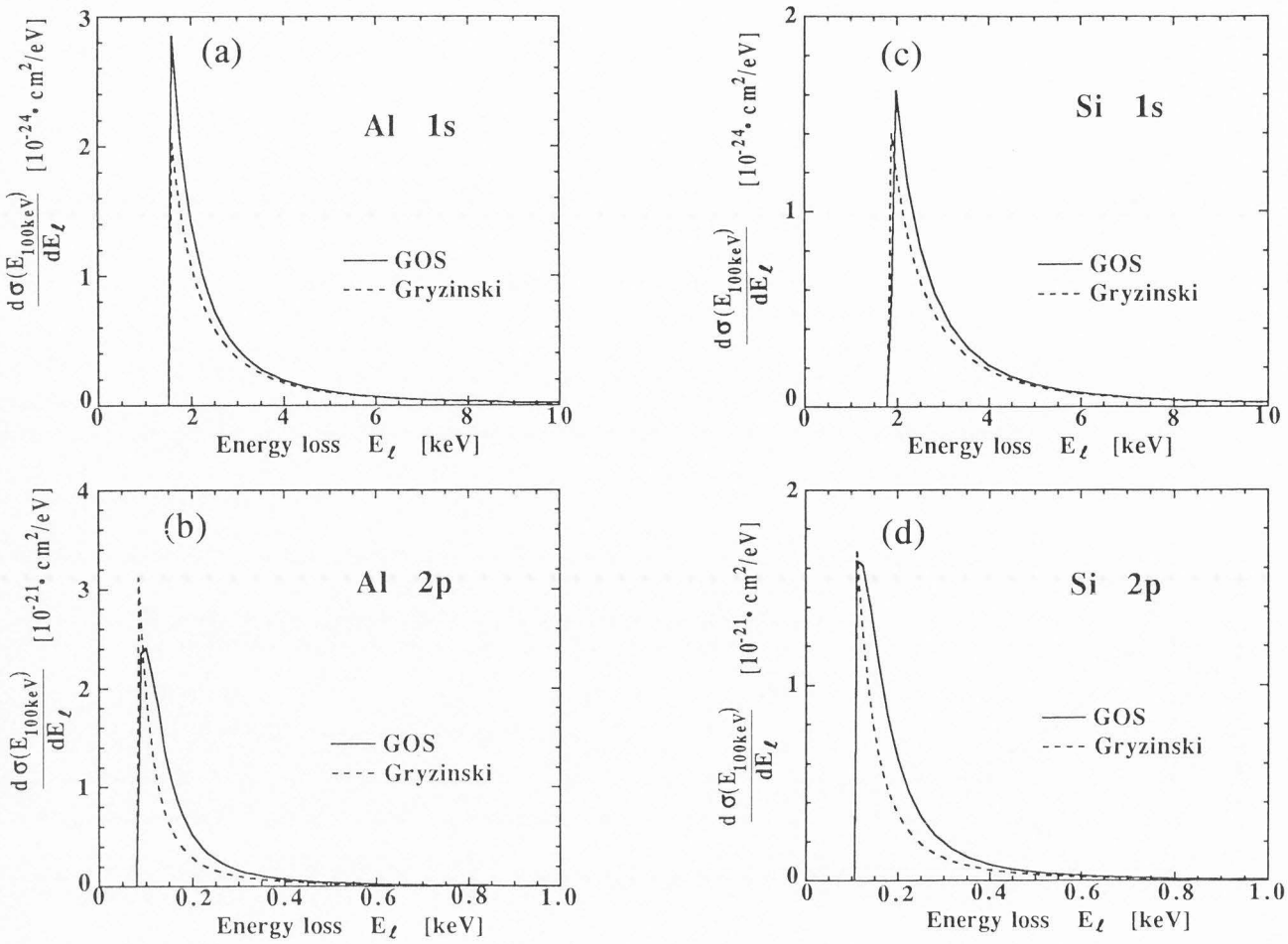

Figure 3. Differential cross-sections with electron energy loss at ionizations of (**a**) Al-1s, (**b**) Al-2p, (**c**) Cu-1s, and (**d**) Cu-2p electrons. The energy of the primary electron is 100 keV. The results obtained by the GOS is compared with the results obtained by the Gryzinski equation.

The GOS is a function of both the energy E_l and the momentum k supplied to the atom. The two-dimensional plot of the GOS is known as the Bethe surface, and examples for Al-1s and Al-2s electrons are shown in Figure 2. Then, the total ionization cross-section is obtained by an integration of the GOS with both $\ln(ka_0)^2$ and E_l.

In a practical procedure, we employ a one-electron wave function of a single atom. The wave function $P_{nl}(r)$ for each nl-shell is a solution to the radial Schrödinger equation with a central potential $U(r)$:

$$\left(\frac{d^2}{dr^2}+U(r)+\varepsilon_{nl}-\frac{l(l+1)}{r^2}\right)P_{nl}(r)=0, \qquad (5)$$

where the energy is expressed in Rydberg units, and the distance is expressed in Bohr units. The eigen function $P_{nl}(r)$, the eigen value, and the atomic potential of the initial ground state are obtained using the Hartree-Slater calculation, which has originally been done by Herman and Skillman [6]. ε_{nl} is the eigen energy of nl-th sub-shell electrons, and the value is always negative. The eigen function of inner-shell electrons and the atomic potential are used as the initial state for the following ionization process.

In the final state, the inner-shell electron is free from the atom and has a certain energy in a continuum state, and the primary electron is also away from the atom. The wave function of this state is calculated numerically from the Schrödinger equation. For the ionization process in which an electron in the nl-th sub-shell goes to a continuum $\varepsilon l'$ state, we calculated the following radial Schrödinger equation under the same central potential $U(r)$:

$$\left(\frac{d^2}{dr^2}+U(r)+\varepsilon-\frac{l'(l'+1)}{r^2}\right)P_{nl'}(r)=0 \qquad (6)$$

where ε is the energy of the ionized electron at the continuum state, and the value is positive. We solved this equation by the Runge-Kutta method [20] and obtained the normalized wave function at the final state.

By integrating the matrix elements of these wave functions of the initial and the final states as expressed by eq. (2), the GOS and the ionization cross-section are obtained. In order to carry out the integration of the form factor of eq. (2) we use the expansion of a plane wave in terms of the Bessel functions. The result is,

$$\left|F_{n l,\varepsilon l'}(k)\right|^2 = (2\,l'+1)\sum_{\lambda}(2\,\lambda+1)\left[R^{\lambda}_{n l,\varepsilon l'}(k)\right]^2\left|\begin{pmatrix} l' & \lambda & l \\ 0 & 0 & 0 \end{pmatrix}\right|^2 \tag{7}$$

where

$$R^{\lambda}_{n l,\varepsilon l'}(k) = \int_0^{\infty} P_{n l}(r)\, j_{\lambda}(k\,r)\, P_{\varepsilon l'}(r)\, d\,r, \tag{8}$$

$j_{\lambda}(kr)$ is the λ-th Bessel function, and is Wigner's 3-j symbol [18]. Using these equations, the GOS and the ionization cross-section are expressed in the following equations:

$$f_{n l,\varepsilon}(k) = (\varepsilon - \varepsilon_{n l})\,(k\,a_0)^{-2}\sum_{l'=0}^{\infty}\left|F_{n l,\varepsilon l'}(k)\right|^2 \tag{9}$$

$$\sigma_{n l,\varepsilon l'} = \frac{8\,\pi a_0^2}{m\,v^2/\Re}(2\,l'+1)\sum_{\lambda}(2\,\lambda+1)\left|\begin{pmatrix} l' & \lambda & l \\ 0 & 0 & 0 \end{pmatrix}\right|^2 \times \int_{\ln(k_{\min}a_0)^2}^{\ln(k_{\max}a_0)^2}\frac{\left[R^{\lambda}_{n l,\varepsilon l'}(k)\right]^2}{(k\,a_0)^2}\, d\ln(k\,a_0)^2 \tag{10}$$

The GOS is a function of both the energy transfer and the momentum transfer to the atom. The measurable ionization cross-section for a fixed energy transfer is the sum of the above cross-sections over all final angular momenta l' as follows:

$$\sigma_{n l,\varepsilon} = \sum_{l'=0}^{\infty}\sigma_{n l,\varepsilon l'} \tag{11}$$

Results and Discussion

The ionization cross-sections

Figures 3a-3d show the differential cross-sections with electron energy loss at ionizations of Al-1s, Al-2p, Cu-1s, and Cu-2p electrons, respectively. For comparison, the cross-section of the classical Gryzinski equation [2] is also plotted in broken lines. The data obtained by these two methods are fairly close. As we integrate this cross-section for all energy losses, the total ionization cross-section for ionization of all *nl*-shell electrons is obtained. Figures 4a-4c show a comparison between the total cross-sections obtained by GOS and the Gryzinski equation for 1s, 2s, and 2p electrons of Al, Si, and Cu. Although some efforts have been made to summarize this

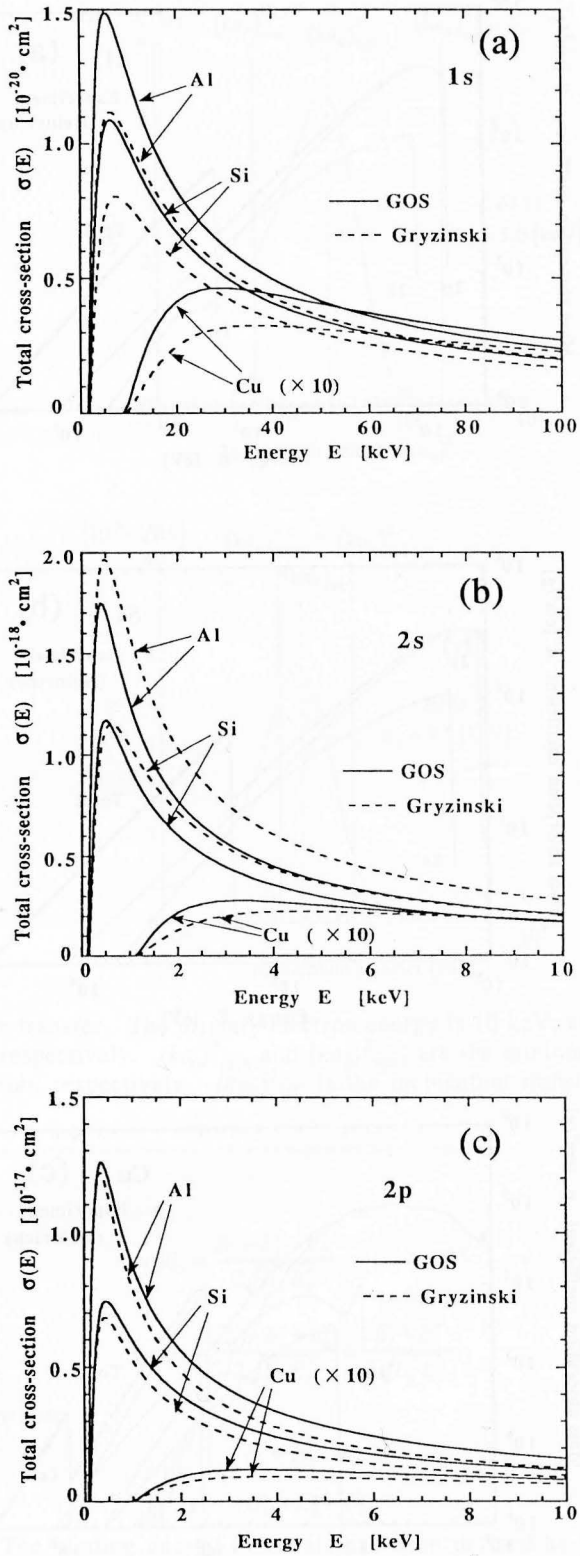

Figure 4. Total ionization cross-section for (**a**) 1s, (**b**) 2s, and (**c**) 2p electrons of Al, Si, and Cu atoms. Comparison between the results obtained by the GOS and the Gryzinski equation is made.

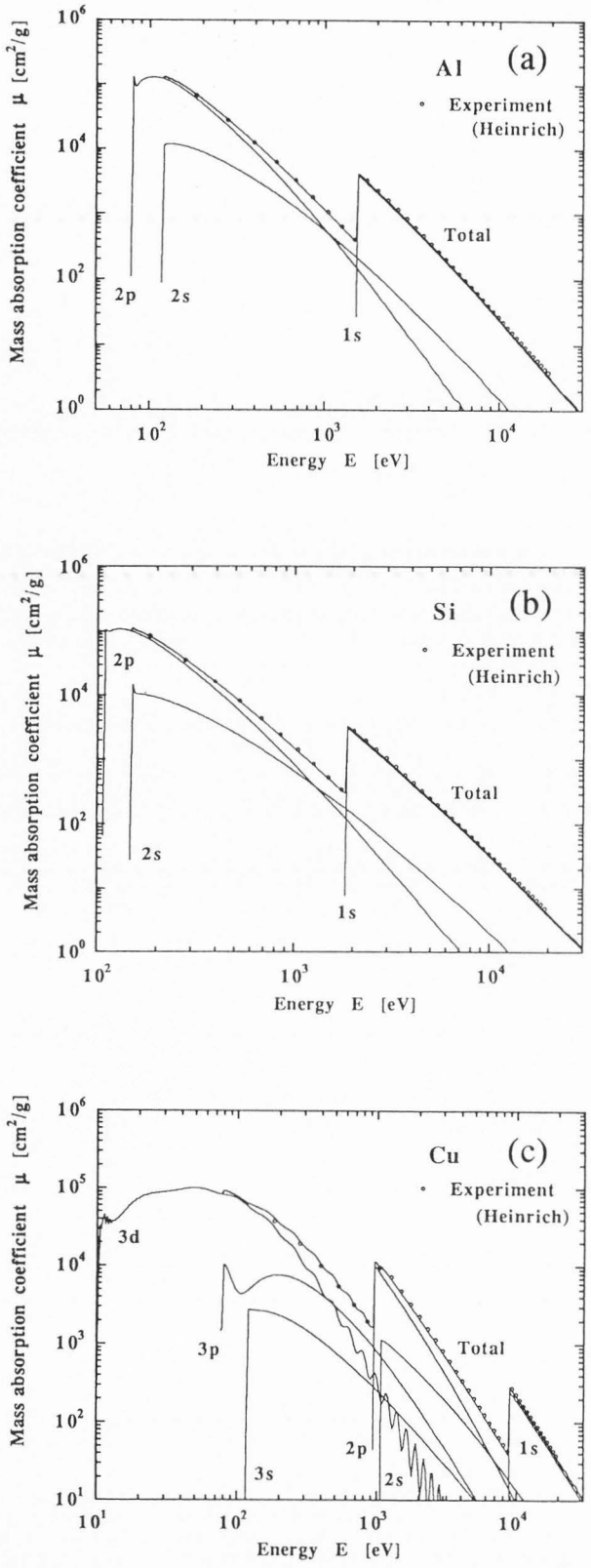

Figure 5. Photo-absorption coefficient obtained by the GOS is compared with the experimental data for Al, Si, and Cu.

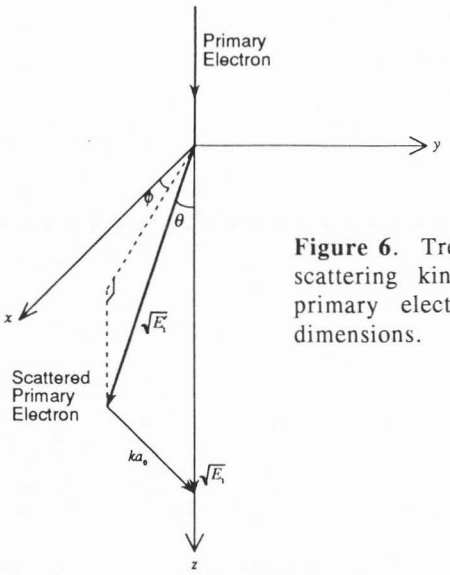

Figure 6. Treatment of the scattering kinematics of a primary electron in three dimensions.

difference [14] the difference shows almost no systematic characteristics with neither the atomic number nor the kind of the sub-shell.

Optical absorption of inner-shell electrons

The photo-ionization cross-section for all *nl*-shell resulting in an ejected electron of energy ε at a continuum state is given by the zero-k limit of the GOS,

$$\sigma_{opt} = \frac{\pi e^2 h}{m c} \lim_{k \to 0} f_{n l, \varepsilon}(k) \qquad (12)$$

Equation 12 gives the dipole oscillator strength (DOS), which is proportional to the X-ray absorption coefficient [4, 13]. For an electron energy below around 100 keV, contributions of the Compton effect and pair production can be neglected, and the photo-ionization is the major process of the X-ray absorption, for atoms with not very high atomic numbers. Several experimental results of the coefficient have been reported. In Figures 5a-5c, the photo-absorption coefficients obtained by the GOS are shown for Al, Si and Cu. Here, we compare the results with the recent data of Heinrich [5], who gave empirical equations to fit all reliable experimental data available for a variety of elements. Not only the total absorption, but also the contribution of each sub-shell is plotted. The absorption jump can be clearly attributed to each sub-shell's absorption edge. It is found that the contribution of the Cu-3d electron ionization shows a wavy structure. It is because of a problem in our numerical calculation, and it is not essential. Although the comparison is made in a logarithmic scale and details are not always clear, the agreement is very good in a wide range of X-ray energies.

Scattering kinematics

Suppose that a primary electron with a kinetic energy of E_1 has an inelastic collision with an inner-shell electron of a kinetic energy at E_2, and loses an energy E_l and transfers a momentum ka_0. Here, the energy of the scattered primary electron is E_1', and the energy of the

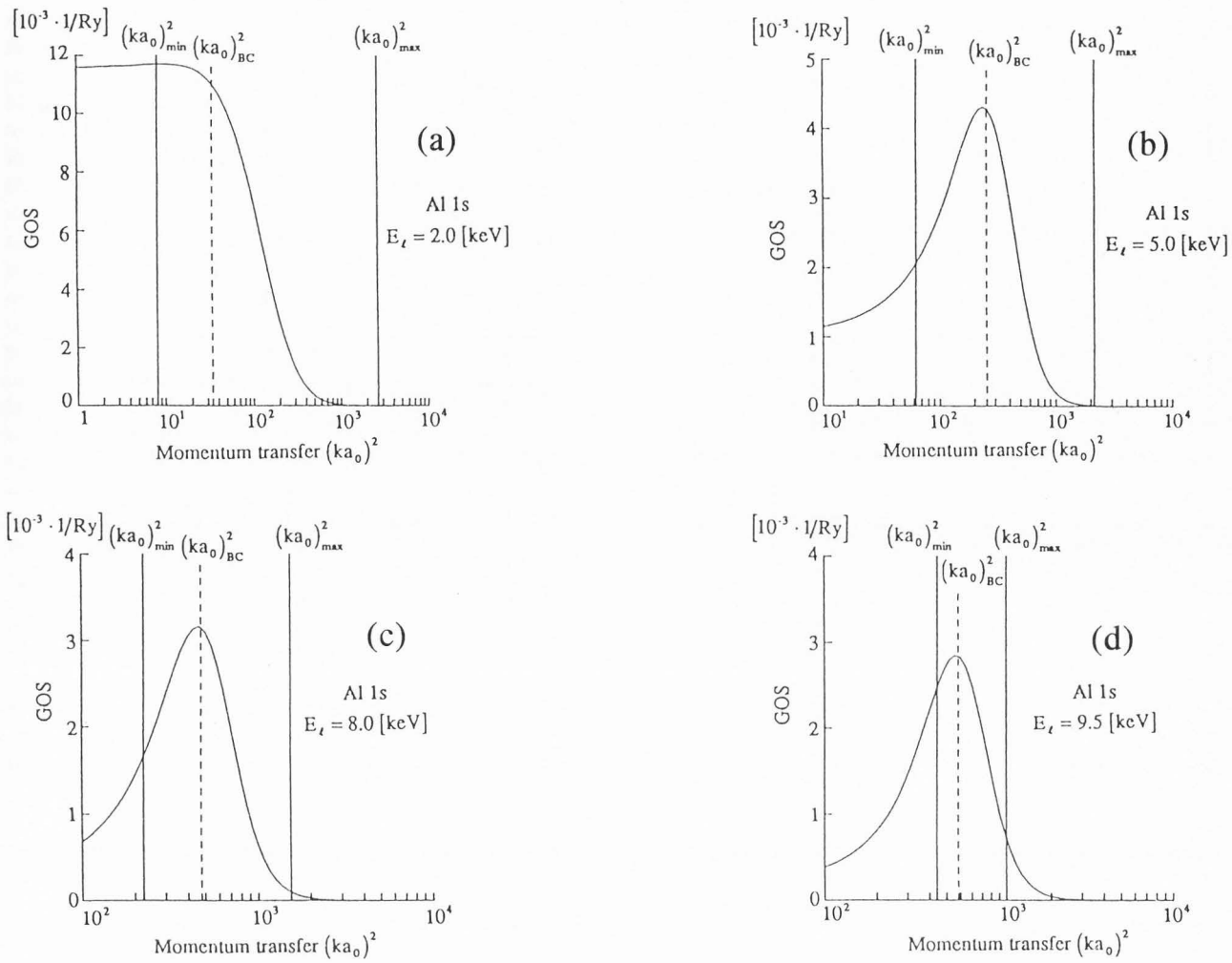

Figure 7. The GOS distribution as a function of the momentum transfer. The primary electron energy is 10 keV, and the energy loss is 2, 5, 8, 9.5 keV for (**a**), (**b**), (**c**), and (**d**), respectively. $(ka_0)^2_{\min}$ and $(ka_0)^2_{\max}$ are the minimum and the maximum momentum transfers available at the collision, respectively. $(ka_0)^2_{BC}$ is the momentum transfer obtained by the classical binary collision model.

generated secondary electron is E_2'. If the electron to be scattered is weakly bound by an atom, the scattering angle can be calculated from momentum conservation law. According to the kinematics of this scattering, the scattering angle of the primary electron θ_1 at the ionization of inner-shell electrons is obtained by the following equation:

$$\cos\theta_1 = \frac{E_1 + E_1' - (ka_0)^2}{2\sqrt{E_1 E_1'}} \tag{13}$$

The coordinate is taken as illustrated in Figure 6. If we assume that the term $(ka_0)^2$ is the result of the energy transfer from the primary electron to the secondary electron in a situation of momentum conservation, as expressed by $(ka_0)^2 = E^2$', the following formulation can be made:

$$\cos\theta_1 = \frac{E_1 + E_1' - E_2'}{2\sqrt{E_1 E_1'}} \tag{14}$$

$$\cos\theta_2 = \frac{E_1 - E_1' + E_2'}{2\sqrt{E_1 E_2'}} = \frac{E_\ell + E_2'}{2\sqrt{E_1 E_2'}} \tag{15}$$

where

$$E_1' = E_1 - E_\ell \tag{16}$$

$$E_2' = E_\ell - E_B \tag{17}$$

The binding energy in metals has been defined as the energy needed to raise an electron to the Fermi level, rather than to the vacuum level. For a consideration of the Fermi energy in a simulation of electron scattering in metals, one can use the relation of $E_2' = E_l - E_B + E_F$.

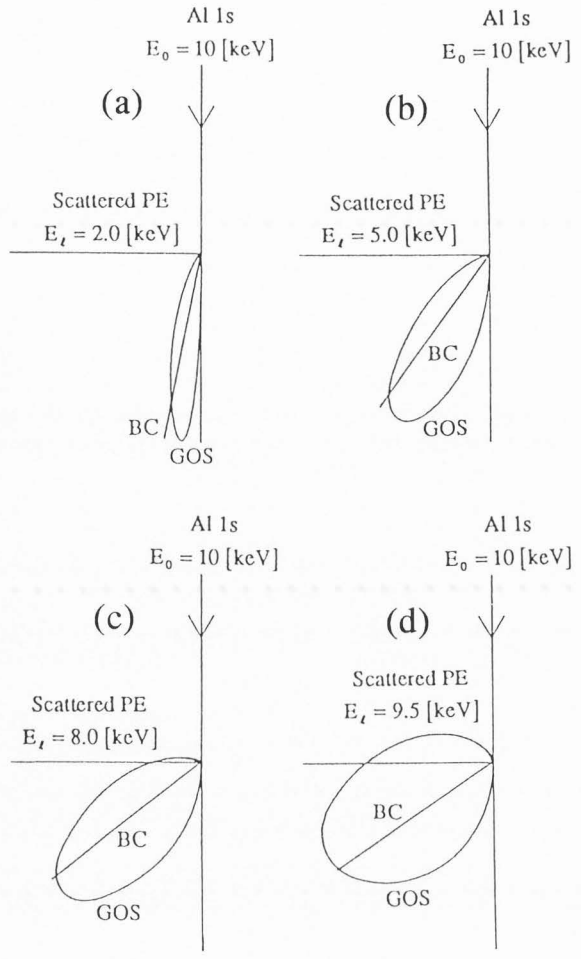

Figure 8. Scattering angle distribution of the primary electrons at the collision. Each distribution from (**a**) to (**d**) corresponds to the energy transfer shown in Figure 7. The label "GOS" shows the distribution obtained by the GOS, and "BC" shows the angle obtained by the classical binary collision model.

The expressions of eqs. (14)-(17) are frequently used in electron scattering simulations, as the result of the classical binary collision model or the classical binary encounter approximation. If an electron to be scattered is free, that is $E_B = 0$, the energy conservation law can be applied. Then, the angle between two scattered electrons, that is $\theta_1 + \theta_2$, derived by eqs. (14) and (15) after the collision is 90°. The maximum scattering angle of the primary electron is 90°. One substantial characteristics of this analysis is that the scattering angle is fixed to be only one direction for a certain energy transfer.

On the other hand, in the present treatment of the scattering using the GOS, we can use the relation between the energy and the momentum transfers, as expressed by the Bethe surface [8], and full use of eq. (13) is possible in this treatment. The angular distribution of the primary electrons is obtained at the fixed energy loss. As expressed in eq. (1) the momentum transfer is limited because the scattering angle of the primary electron is between 0 to π. In other words, scattering angle distributes from 0 to π for a fixed energy transfer. Figure 7 shows the GOS as a function of the momentum transfer at energy loss E_l of 2.0, 5.0, 8.0 and 9.5 keV for 10 keV primary electrons after Al-1s electron ionization. k_{min} and k_{max} are the minimum and the maximum momentum transfer at the collision, respectively. $(ka_0)^2_{BC}$ is the momentum transfer calculated by the classical binary collision model with eqs. (14) and (15). It is shown that $(ka_0)^2_{BC}$ agrees well with the maximum of the GOS distribution for relatively high energy loss.

Figure 8 shows an angular distribution of the scattered primary electrons. The distribution is shown in a polar plot corresponding to the scattering shown in Figure 7. The intensity is in arbitrary unit. The figure also shows the scattering angles obtained by the classical binary collision model, and the angles are calculated by eqs. (14) and (15). As found in the figure, the intensity obtained by the GOS distributes around the angle given by the classical model. In order to obtain these distributions, the GOS distributions are multiplied by $2\pi\sin\theta$ for a given scattering angle θ. That is the reason why the intensities at zero radian and at π radian are zero. It is also the reason why although the most probable momentum transfer of the GOS agrees with that of the classical binary collision model, the most probable scattering angles do not always agree.

Not only the scattering angle distribution for the primary electrons, but also the distribution for the secondary electrons generated by the collision may be derived, if the initial energy and the momentum of the inner-shell electron at the ground state is known. It is possible to assume these intial conditions using the radial wave function and the radial potential distribution of the inner-shell electron given above. Therefore, the initial state of an inner-shell electron may be given statistically by the probability function, and this problem may be solved by the Monte Carlo method. This method gives a reasonable extension of the classical treatment on the angular distribution based on the quantum-mechanical treatment. However, this is approximately valid for a quasi-free scattering, in which the binding of a struck electron is almost negligible. The right expression of the scattering angle distribution of the ionized electrons should contain the phase-shift difference as expressed by Manson *et al.* [16], and not just the GOS. They have derived the triple differential cross-section, that is, differential in the energy of the ionized electron, differential in the direction of the ionized electron, and differential in the direction of the scattered primary electron.

Conclusions

For a quantitative discussion of an angular resolved electron energy loss spectrum, it should be necessary to treat precisely the scattering kinematics of

incident primary electrons and the scattered electrons. Here, the generalized oscillator strength is introduced in the inner-shell electron ionization process. The Hartree-Slater atomic potential we used as the initial ground state of an atom is close to the Hartree-Fock atomic potential. The differential cross-section and the total cross-section derived from the generalized oscillator strength are evaluated by a comparison with the data obtained by the Gryzinski equation. The photo-absorption cross-section obtained by the generalized oscillator strength is also evaluated by a comparison with experimental data, and the agreement is very good in a wide range of photon energy. Taking into account both the energy and the momentum transfers at the ionization of inner-shell electrons, the scattering angle distribution of the primary electron is described. The intensity distributes around the angle given by the classical binary collision model. The most probable angle at the distribution almost agrees with the angle which is given by the classical model. In order to interpret characteristic variations of the practical energy loss spectrum or that of the angular distribution of the scattered electrons, the present treatment is much preferable rather than the classical model.

References

1. Ahn C, Rez P. (1985). Inner shell edge shapes in electron energy loss spectroscopy. Ultramicrosc. **17**, 105-115.

2. Ding ZJ, Shimizu R. (1988). Monte Carlo study of backscattering and secondary electron generation. Surf. Sci. **197**, 539-554.

3. Ganachaud JP, Cailler M. (1979). A Monte-Carlo calculation of the secondary electron emission of normal metals. Surf. Sci. **83**, 498-530.

4. Goldberg SM, Fadley CS, Kono S. (1981). Photoionization cross-sections for atomic orbitals with random and fixed spatial orientation. J. Electron Spectrosc. Relat. Phenome. **21**, 285-363.

5. Heinrich KFJ. (1986). Mass absorption coefficients for electron probe microanalysis. In: Proc. 11th Intn. Cong. on X-Ray Optics and Microanalysis. Brown JD, Packwood RH (eds.). Univ.Western Ontario, London, Canada. 67-119.

6. Herman F, Skillman S. (1963). Atomic Structure Calculations. Prentice-Hall, Englewood Cliffs, NJ.

7. Jolly WL, Bomben KD, Eyermann CG (1984). Core electron binding energies for gaseous atoms and molecules. Atomic Data and Nuclear Data Tables **31**, 433-493.

8. Inokuti M. (1971). Inelastic collisions of fast charged particles with atoms and molecules - The Bethe theory revisited. Rev. Mod. Phys. **43**, 293-347.

9. Koshikawa T, Shimizu R. (1974). A Monte Carlo calculation of low-energy secondary electron emission from metals. J. Phys. **D7**, 1303-1315.

10. Kotera M. (1989). A Monte Carlo simulation of primary and secondary electron trajectories in a specimen. J. Appl. Phys. **65**, 3991-3998.

11. Kotera M, Ijichi R, Fujiwara T, Suga H, Wittry DB. (1990). A simulation of electron scattering in metals. Jpn. J. Appl. Phys. **29**, 2277-2282.

12. Kotera M, Yamamoto K, Suga H. (1992). Application of a direct simulation of electron scattering to quantitative electron-probe microanalysis. In: Microbeam Analysis 1992. San Francisco Press. 1670-1671.

13. Leapman RD, Rez P, Mayers DF. (1980). K, L, and M shell generalized oscillator strengths and ionization cross-sections for fast electron collisions. J. Chem. Phys. **72**, 1232-1243.

14. Luo S, Joy DC. (1991). Calculations of X-ray ionization cross-sections at low overvoltage ratios. In: Microbeam Analysis 1991. San Francisco Press. 67-68.

15. Manson ST. (1972). Inelastic collisions of fast charged particles with atoms: Ionization of the aluminum L shell. Phys. Rev. **A6**, 1013-1024.

16. Manson ST, Toburen LH, Madison DH, Stolterfoht N. (1975). Energy and angular distribution of electrons ejected from helium by fast protons and electrons: Theory and experiment. Phys. Rev. **A12**, 60-79.

17. McGuire EJ. (1971). Inelastic scattering of electrons and protons by the elements He to Na. Phys. Rev. **A3**, 267-279.

18. Messiah A. (1966). Quantum Mechanics, vol. 2. North-Holland, Amsterdam. 1054-1056.

19. Murata K. (1974). Spatial distribution of backscattered electrons in the scanning electron microscope and electron microprobe. J. Appl. Phys. **45**, 4410-4417.

20. Newbury ACR. (1974). Handbook of Applied Mathematics. Van Nostrand Reinhold, New York. 1035-1036.

21. Reimer L, Krefting ER. (1976). The effect of scattering models on the results of Monte Carlo calculation. National Bureau of Standards, Washington DC, Spec. Pub. **460**, 45-60.

22. Rez P. (1984). Electron ionization cross-sections for K, L and M shells. X-ray Spectr. **13**, 55-59.

23. Scofield JH. (1978). K- and L-shell ionization of atoms by relativistic electrons. Phys. Rev. **A18**, 963-970.

24. Strand TG, Bonham RA. (1964). Analytical expressions for the Hartree-Fock potential of neutral atoms and for the corresponding scattering factors for X-rays and electrons. J. Chem. Phys. **40**, 1686-1691.

Discussion with Reviewers

P. Rez: How are the continuum wave functions normalized?

Authors: The normalization procedure we used is the same as the Mason's procedure [15]. Details of this procedure is written in the Appendix in the paper: Cooper JW (1962). Photoionization from outer atomic sub-shells. A model study. Phys. Rev. **128**, 681-693; with a corrected expression by: Manson ST, Cooper JW. (1968). Photo-ionization in the soft X-ray range: Z-dependence in a central-potential model. Phys. Rev.

165, 126-138.

F. Hasselbach: Assume that we are interested in the spatial distribution of backscattered electrons or secondary emission from the surface of a bulk specimen. How large are the modifications caused by your sophisticated calculation when you compare your results with those obtained by the single scattering model?
Authors: The largest difference of the present treatment from the single scattering model, using the classical binary collision model, is in whether the scattering angle at a fixed energy loss shows a distribution or not. In another situation, the difference is in whether the energy loss at a fixed scattering angle has a spectrum or not. In Figure 8 we have shown the relative amplitude of the angular distribution in a polar plot. If we are interested in the angular distribution or the energy distribution of singly scattered electrons at the specimen surface, the influence of the difference is significant. However, if we are interested in the backscattered electrons which have been produced by multiple collisions in a solid with a various types of inelastic scattering, the influence of the difference discussed above may be negligible.

H. Niedrig: What changes are to be expected for atoms of higher atomic numbers than Z = 29 (Cu)?
Authors: As discussed in the text, the difference in the ionization cross-section obtained by the GOS and that obtained by the Gryzinski equation shows almost no systematic characteristics with neither the atomic number nor the kind of the sub-shell. It is difficult to summarize or to guess this difference as a function of the atomic number, and one has to calculate in each case.